Electron magnetohydrodynamic turbulence in a high-beta plasma. I. Plasma parameters and instability conditions

R. L. Stenzel and J. M. Urrutia[a)]
Department of Physics and Astronomy, University of California, Los Angeles, California 90095-1547

(Received 24 November 1999; accepted 4 May 2000)

The interaction of a dense discharge plasma with a weak external magnetic field has been studied experimentally. The electron pressure exceeds the field pressure and forms a magnetic hole in the plasma interior. The ions are unmagnetized, while the electrons are in a transition regime from none to full magnetization. The electron confinement changes from Boltzmann equilibrium to magnetic confinement. The pressure balance equation does not describe the diamagnetism because ambipolar $\mathbf{E}\times\mathbf{B}$ drifts oppose the diamagnetic drift. The net drift exceeds the sound speed by an order of magnitude and produces a strong two-stream cross-field instability. Although its spectrum is close to the lower hybrid instability, there are significant differences from the classical lower hybrid instability, e.g., the presence of strong magnetic fluctuations. These fall into the regime of electron magnetohydrodynamics (EMHD) with unmagnetized but mobile ions. While the EMHD turbulence is the main focus of the two following companion papers, this first paper describes the plasma diamagnetism and basic parameters that lead to the instability. © *2000 American Institute of Physics.* [S1070-664X(00)03111-6]

I. INTRODUCTION

The interaction of plasmas and magnetic fields is of fundamental interest in space and laboratory plasma physics. Dense hot plasmas exhibit a significant diamagnetism, which changes the magnetic field inside the plasma. A quantitative measure for this effect is the plasma ''beta,'' which is the ratio of the particle pressure to the external magnetic field pressure, $\beta=nkT/(B_0^2/2\mu_0)$.[1] However, the notion of a ''high''-β plasma may depend on the phenomenon of interest: Wave phenomena can change for $\beta\simeq m_e/m_i\ll 1$,[2] the economics of magnetic fusion devices requires $\beta\approx 10\%$,[3] magnetic holes can be formed in space plasmas with β of order unity,[4,5] and extremely high-β plasmas such as the solar interior ($\beta>10^5$) can completely deform or confine magnetic fields.[6] In the present work, we deal with laboratory plasmas where $\beta>1$ and describe diamagnetism and associated instabilities in the presence of pressure and field gradients. Major findings are that electron magnetohydrodynamics (EMHD)[7] can govern the plasma physics near a magnetic bubble, i.e., the diamagnetism essentially demagnetizes the ions, while leaving the electrons still magnetized. In this parameter regime, a strong instability develops due to the electron diamagnetic drift through the unmagnetized slow ions. Such current-driven cross-field instabilities, observed earlier in plasmas with $\beta<1$,[8] produce large-amplitude density fluctuations near the lower hybrid frequency that propagate at approximately the sound speed in the direction of the electron diamagnetic drift. However, due to the high-β which couples density to magnetic field fluctuations, and the dependence on the temperature ratio $T_e/T_i\gg 1$, the instability is not described by a classical lower hybrid drift wave,[9–11] a cross-field ion instability,[12] or an $\mathbf{E}\times\mathbf{B}$ drift wave instability with unmagnetized ions[13] or magnetized ions.[14] However, it does have the basic characteristics of a drift dissipative instability.[15]

Another important result is that the pressure balance equation used in MHD, $B_{\text{plasma}}^2/2\mu_0+nkT_e=B_0^2/2\mu_0=\text{const}$,[16] does not hold when $B_{\text{plasma}}\to 0$ and the electron confinement changes from magnetic force balance to Boltzmann equilibrium.[1] In this transition regime, the diamagnetic drift is opposed by an $\mathbf{E}\times\mathbf{B}$ drift which reduces the diamagnetic field change. If the electric field equals the ambipolar field, $\mathbf{E}=-\nabla(nkT_e)/ne$, the net drift, hence the diamagnetism, would vanish. Observations show that the average magnetic field inside the plasma column is fully expelled for $\beta\approx 5$ rather than for $\beta=1$. Likewise, the ratio of normalized magnetic and density fluctuations is smaller than expected from the pressure balance equation, $|\delta B/B|<\beta/2|\delta n/n|$. These basic features of a bounded high-β plasma are described in this work, Part I of three companion papers. Basic instability properties such as frequency spectra, correlations, and amplitude distributions are also presented. Part II[17] describes in detail the features of the instability as obtained from single-point measurements. These include cross-correlations between density and magnetic field fluctuations, amplitude distributions showing wave steepening and current sheet formation, and magnetic hodograms showing that the magnetic fluctuations have the properties of low frequency oblique whistlers. Finally, in Part III[18] the three-dimensional (3D) space–time properties of the instability are described from conditionally averaged multipoint measurements. The average direction and speed of propagating density and magnetic field fluctuations are obtained. It is shown there that the density fluctuations form flutelike perturbations propagating along the mean isobars at sonic speeds, that the magnetic

a)Electronic mail: urrutia@physics.ucla.edu

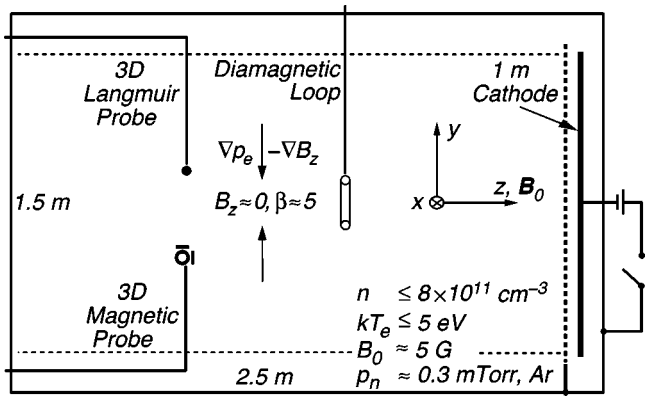

FIG. 1. Experimental setup with basic plasma parameters.

field and current density form flux ropes of negative self helicity, and that it is possible to reconstruct the ''instantaneous'' magnetic field lines, current density lines, and single particle orbits in a turbulent high-β plasma.

The present Part I is organized as follows: After describing in Sec. II the experimental setup and measurement techniques, the experimental results are presented in Sec. III, divided into various subsections. The conclusion, Sec. IV, points out the relevance of the present findings to related observations and applications.

II. EXPERIMENTAL ARRANGEMENT

The experiments are performed in a large linear plasma device (1 m diam$\times$2.5 m length) schematically shown in Fig. 1. A uniform axial dc magnetic field $B_0=5$ G is applied. A pulsed discharge ($V_{\rm dis}\simeq 60$ V, $I_{\rm dis}\simeq 750$ A, $t_{\rm pulse}\simeq 4$ ms, $t_{\rm rep}\simeq 1$ s) of density $n\leqslant 8\times10^{11}$ cm^{-3}, electron temperature $kT_e\leqslant 5$ eV is produced in Argon at a pressure $p_n\simeq 0.3$ mTorr using a 1 m diam oxide-coated cathode.[19] The cathode emission is made nonuniform so as to produce a strong radial density and temperature gradient.

The plasma parameters $(n,kT_e,\phi_{\rm pl})$ are measured with a small Langmuir probe (1 mm$\times$1.5 mm) movable in 3D space. Other Langmuir probes movable in one dimension (1D) are also used to record electron/ion saturation currents and their fluctuations. The validity of Langmuir probe measurements in weakly magnetized plasmas has been checked earlier via independent diagnostics with electron plasma waves,[20] ion acoustic waves,[21] and whistler waves.[22] Time-varying magnetic fields are measured with a magnetic probe consisting of three orthogonal, electrostatically shielded loops (1 cm diam, 30 turns), which provide (B_x,B_y,B_z) simultaneously versus time ($\sim$10 ns resolution) at a given position $\mathbf{r}$. The probe voltages ($V_{\rm probe}\propto -dB/dt$) are integrated either by analog techniques (operational amplifier) or digitally (digital oscilloscope/computer). The probe is calibrated in a known magnetic field configuration. The spatial distribution of $\mathbf{B}(\mathbf{r},t)$ is obtained by repeating the pulsed discharges and slowly varying the probe position in a 3D volume ($\sim$1 cm resolution). Fluctuations are analyzed by forming statistical averages over an ensemble of highly reproducible discharge pulses. Using conditional averaging, the typical space–time behavior of the turbulence

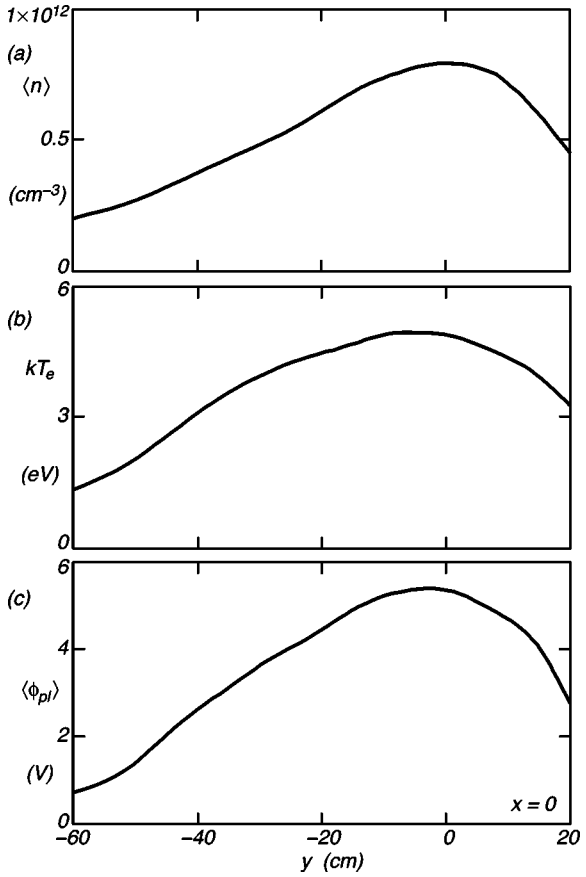

FIG. 2. Radial profiles of average density, electron temperature, and plasma potential during the steady-state phase of the pulsed discharge.

$[\langle n(\mathbf{r},t)\rangle,\langle \mathbf{B}(\mathbf{r},t)\rangle]$ is resolved, which allows identification of the unstable modes.[8] In order to measure the diamagnetic change of the dc magnetic field inside the high-β plasma, a larger loop (6 cm radius, 4 turns, electrostatically shielded) movable in 1D is used.

Typical measurements include swept Langmuir probe traces (sweep speed $\leqslant 10$ μs), digital recording of probe saturation currents and magnetic probe signals, while typical data analysis involves ensemble averages, amplitude distributions, magnetic hodograms, and conditional averaging described in companion papers.[17,18]

III. EXPERIMENTAL RESULTS

A. Plasma parameters and diamagnetism

Typical radial profiles of the time-averaged electron density $\langle n\rangle$, temperature $\langle kT_e\rangle$, and plasma potential $\langle \phi_{\rm pl}\rangle$ during the dc discharge are shown in Figs. 2(a)–2(c). The measurements show the radial gradients of typical scale lengths $|n/\nabla n|\simeq|T_e/\nabla T_e|\simeq 80$ cm and the presence of a radial electric field $E_r=-\nabla\phi_{\rm pl}\leqslant 0.1$ V/cm which was not observed at higher magnetic fields, $B_0\simeq$ 15 G.[8] Axial gradients are negligible compared to the radial gradients. Axially, the electrons are completely reflected by the cathode sheath, and partly reflected by the smaller anode sheath. The radial electric field and the anode sheath self-consistently balance the electron and ion fluxes. The ion temperature in partially ion-

TABLE I. Basic plasma parameters.

Electron density	$n_e = 5\times10^{11}$ cm^{-3}
Electron temperature	$kT_e = 4$ eV
Electron plasma frequency	$\omega_{pe}/2\pi \simeq 6.4$GHz
Electron cyclotron frequency	$\omega_{ce}/2\pi \simeq 14$ MHz
Lower hybrid frequency	$\omega_{\rm LH} = (\omega_{ce}\omega_{ci})^{1/2}/2\pi \simeq 52$ kHz
Electron cyclotron radius	$r_{ce} \simeq 1.4$ cm
Electron-ion collision frequency	$\nu_{ei} \simeq 1.8\times10^6$ s^{-1}
Electron mean free path	$\lambda_{ei} \simeq 66$ cm $< \lambda_{en}$
Electron cyclotron radius	$r_{ce} \simeq 1.4$ cm
Normalized electron collision frequency	$\nu_{ei}/\omega_{ce} \simeq 0.02$
Ion cyclotron frequency	$\omega_{ci}/2\pi \simeq 190$ Hz
Ion cyclotron radius	$r_{ci} \simeq 120$ cm
Ion-neutral charge-exchange collision frequency (Ref. 23)	$\nu_{in} \simeq 5\times10^3$ s^{-1} ($kT_i \simeq 0.4$ eV)
Ion mean free path	$\lambda_{in} \simeq 28$ cm
Normalized ion collision frequency	$\nu_{in}/\omega_{ci} \simeq 4$

ized discharge plasmas is typically an order of magnitude smaller than the electron temperature.[20] Thus β is essentially determined by the electron pressure. From the measured plasma parameters (5×10^{11} cm^{-3}, 4 eV, 5 G) one can calculate the basic plasma parameters. They are listed in Table I.[23] Additionally, in dc discharges there also exists a population of energetic electrons ($\sim$60 eV) with long collisional mean free path ($\lambda_e > L_{\rm device} = 2$ m), but short scattering distance ($\sim 10 v_e/f_{pe} \simeq 1$ mm) due to the beam-plasma instability near the cathode.[24]

The plasma parameters indicate that the peak electron pressure $nkT_e \simeq 5\times10^{-7}$ J/cm^3 greatly exceeds the external magnetic field pressure $B_0^2/2\mu_0 \simeq 1\times10^{-7}$ J/cm^3, suggesting that for $\beta_e \simeq 5$ the electron diamagnetism entirely expels the external magnetic field. This is confirmed by magnetic loop measurements presented in Fig. 3 as ensemble averages over 200 shots. For reference, Fig. 3(a) shows the time dependence of the pulsed plasma production and decay as indicated by the ion saturation current to a Langmuir probe ($I_{i,\rm sat} \propto n_e\sqrt{kT_e}$). The plasma parameters achieve steady-state values at $t \geqslant 2$ ms into the 4 ms long discharge pulse, while in the afterglow the electron pressure is lost within a fraction of 1 ms (further details presented below). The diamagnetic loop signal in the column center is shown in Fig. 3(b). The induced voltage ($V_{\rm loop} = -d\Phi/dt$) indicates a flux change ($\Phi = \int B_z\, da$) during growth and decay of the plasma pressure. Integration of the loop signal yields the change in the magnetic field [$\Delta B_z = -\int V_{\rm loop}\, dt/(N\pi r^2)$ or 1 G/4.5 μV s for $N = 4$ turns and $r = 6$ cm]. When added to the initial value ($B_0 = 5$ G), the time behavior of the internal axial magnetic field inside the plasma, $B_z = B_0 + \Delta B_z$, is obtained and plotted in Fig. 3(c). As expected, the interior of this high-β plasma is essentially field-free. A further check of the validity of the diamagnetic measurements is provided by a loop rotation. Figure 3(d) shows that the measured magnetic field varies sinusoidally with angle α between loop axis and $\mathbf{B}_0$.

The radial dependence of the ensemble-averaged electron pressure $\langle nkT_e\rangle$ and axial magnetic field $\langle B_z\rangle$, measured during the steady-state discharge, is displayed in Fig. 4. As expected, the field is reduced in the high density region of the plasma column. From the radial magnetic field variation one can calculate the current density $J_x \simeq \mu_0^{-1}\,\partial B_z/\partial y \simeq 0.16$ A/cm^2 and the electron drift velocity $v_{\rm d} = -J/ne \simeq 2\times10^6$ cm/s $\gg c_s = (kT_e/m_i)^{1/2} \simeq 3\times10^5$ cm/s. It is interesting to note that the field increases at the plasma edge above the dc field $B_0 = 5$ G indicated by a straight line. Since on the present time scale the total flux inside the highly conducting plasma chamber is conserved, a reduction of the flux in the column center implies a field increase at the plasma edge. A second interesting observation is that the magnetic field is not fully expelled where $\beta = 1$ (see dashed line), implying that the pressure balance equation, $B_z^2/2\mu_0 + nkT_e = B_0^2/2\mu_0$, does not hold. This aspect has been further investigated by measuring the dependence of B_z in the column center for different values of peak plasma β.

The plasma β in Fig. 5 is varied in two ways: (i) the electron pressure is varied with discharge power ($nkT_e \propto V_{\rm dis} I_{\rm dis}$) at a fixed external magnetic field $B_0 = 5$ G; and (ii) the field B_0 is varied at a constant plasma pressure. In either case the magnetic field is not completely expelled at $\beta = 1$ as predicted by the pressure balance equation (see dashed line).

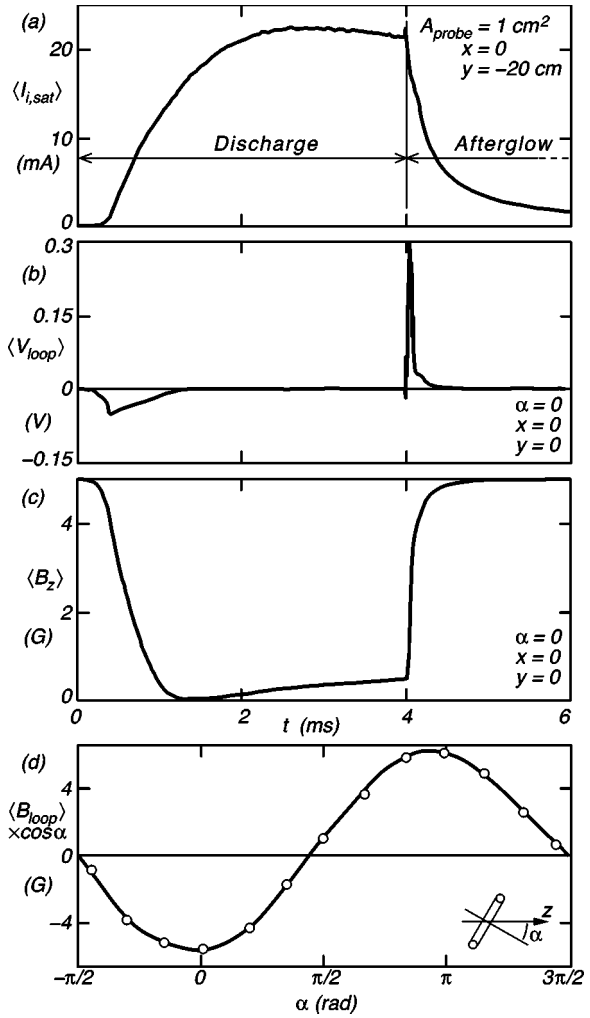

FIG. 3. Measurement of the internal magnetic field in a high-β plasma with a diamagnetic loop. (a) Ion saturation current to a Langmuir probe vs time. (b) Diamagnetic loop voltage. (c) Integrated loop voltage, converted to field strength. (d) Variation of angle α between loop normal and $\mathbf{B}_0$, showing the proper response of a diamagnetic probe.

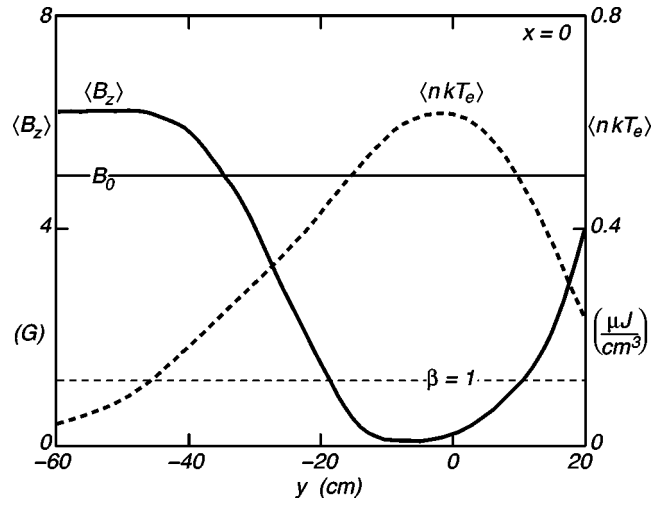

FIG. 4. Radial profiles of the average axial magnetic field $\langle B_z \rangle$ and electron pressure $\langle nkT_e \rangle$, showing the complete field expulsion in the column center. Flux conservation produces a field enhancement ($\langle B_z \rangle > B_0$) at the plasma edge.

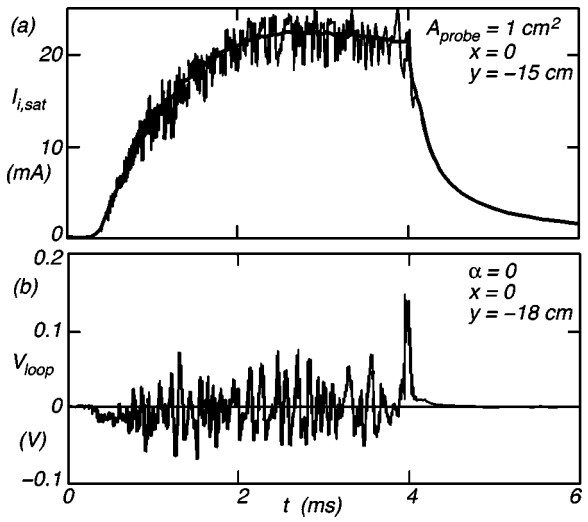

FIG. 6. Fluctuations in density and magnetic field vs time. (a) Ion saturation current for a single discharge and ensemble average (smooth line). (b) Diamagnetic loop voltage, $V_{\rm loop} \propto -\partial B_z/\partial t$.

The reason is that the pressure balance equation applies to a single-fluid MHD plasma where the pressure gradient is balanced only by the magnetic force, $\nabla p = \mathbf{J} \times \mathbf{B}$. An electric field does not exert a net force on a charge-neutral fluid and $\mathbf{E} \times \mathbf{B}$ drifts produce no net currents to alter the magnetic field. However, these conditions do not hold when the ions are unmagnetized while the electrons remain magnetized (EMHD). Now the electron pressure is balanced by *both* magnetic and electric forces, $\nabla p_e = \mathbf{J} \times \mathbf{B} - ne\mathbf{E}$. As β increases and $B \to 0$, a transition from magnetic force balance, $\nabla p = \mathbf{J} \times \mathbf{B}$, to Boltzmann equilibrium, $\nabla p_e = -ne\mathbf{E}$, occurs. The electric field $\mathbf{E} \perp \mathbf{B}$ is directed so as to produce an $\mathbf{E} \times \mathbf{B}$ drift opposing the $\nabla p_e \times \mathbf{B}$ drift. This is readily seen in Fig. 2 where $\mathbf{E} = -\nabla \phi_{\rm pl}$ [Fig. 2(c)] opposes $\nabla p = \nabla nkT_e$ [Figs. 2(a)–2(b)]. Thus the Hall current opposes the diamagnetic current, and the magnetic field inside the plasma is not as low as predicted by the pressure balance equation. Vice versa, $\beta > 1$ is required to completely expel the magnetic field from the plasma. The unmagnetized ions are not confined and drift radially outward along the ambipolar electric field. As long as plasma production can replace the ion loss, a steady-state can be maintained. But if the ion outflow exceeds the neutral inflow the density will decrease, which is noticeable in Fig. 3.

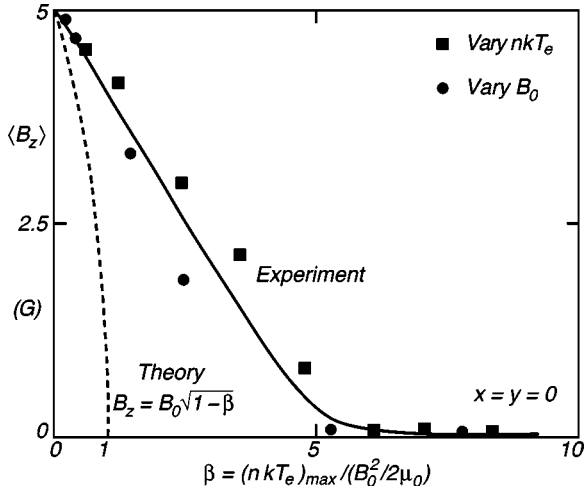

FIG. 5. Variation of the average axial magnetic field $\langle B_z \rangle$ with normalized electron pressure $\beta = \langle nkT_e \rangle / (B_0^2/2\mu_0)$ in the column center. The observations differ from the predictions of the pressure balance equation because both electric and magnetic forces balance the electron pressure.

B. Basic instability properties

The presence of an instability manifests itself in large density and magnetic field fluctuations seen on single shot traces. Figure 6(a) displays the ion saturation current ($I_{i,\rm sat} \propto n$) both for a single discharge pulse (noisy waveform) as well as for an ensemble average of $N = 100$ shots (solid smooth line). Likewise, a single trace of the diamagnetic loop voltage [Fig. 6(b)] indicates strong magnetic fluctuations in B_z, which are not observed in an ensemble average [e.g., Fig. 3(b)]. The fluctuations exhibit no phase coherence from shot to shot, i.e., they are not transient phenomena of the pulsed discharge but an instability. The fluctuations are largest during the discharge and decay rapidly in the afterglow. Details of the decay will be discussed below.

The fluctuation amplitude varies with radial position as shown in Fig. 7. For reference, the radial profile of the electron pressure, nkT_e, is also shown. It is evident that the rms fluctuations in the loop voltage, $V_{\rm loop,rms} = \langle (V_{\rm loop} - \langle V_{\rm loop} \rangle)^2 \rangle^{1/2}$, maximize in the region of the strongest pressure gradients. Density fluctuations show the same behavior. This feature suggests that the instability is excited by the electron diamagnetic drift, $\mathbf{v}_{\rm dia} = \nabla p_e \times \mathbf{B}/neB^2$, through the unmagnetized ions. From Fig. 3 one finds $|n/\nabla n| \simeq 40$ cm and $|T_e/\nabla T_e| \simeq 50$cm, which yields a pressure gradient scale length $L_p = |p_e/\nabla p_e| = (1/40 + 1/50)^{-1} \simeq 22$ cm and a diamagnetic drift speed, $v_{\rm dia} = kT_e/(eBL_p) \simeq 4.6 \times 10^6$ cm/s for $kT_e \simeq 4$ eV and $B_z \simeq 4$ G. This drift is opposed by a smaller $\mathbf{E} \times \mathbf{B}$ drift ($E/B \simeq 2 \times 10^6$ cm/s) resulting in a net drift close

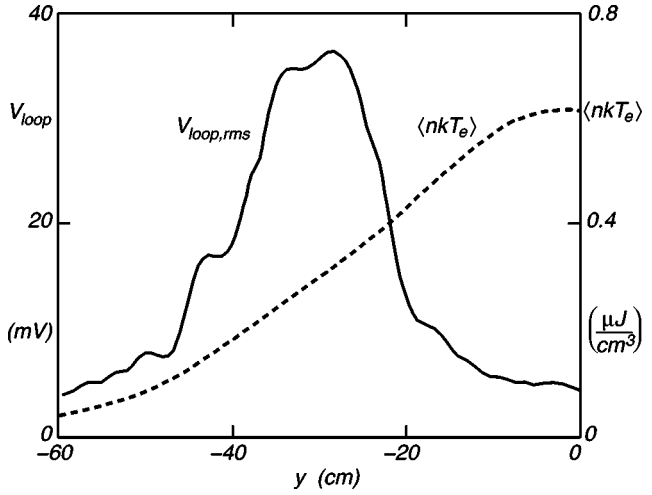

FIG. 7. Radial variation of the magnetic fluctuations ($\propto V_{\text{loop}}$) and of the average electron pressure. The fluctuations maximize in regions of large pressure gradients.

to that derived from the magnetic field measurement. This net drift greatly exceeds the ion sound speed such that the condition for a current-driven cross-field instability is satisfied. Later wave measurements will show that the fluctuations propagate at $v_\perp \approx c_s$ in the electron diamagnetic drift direction.

Frequency spectra and autocorrelations have been determined for magnetic fluctuations measured with the 3D probe, whose dimensions are small compared to the scale length of the fluctuations. Figure 8(a) shows a single-shot trace of $\delta B_z = B_z - \langle B_z \rangle$ versus time, while Fig. 8(b) shows its autocorrelation function, $A(\tau) = \int \delta B_z(t)\, \delta B_z(t-\tau)\, dt$, normalized to its peak value $A(0)$, during the steady-state period of

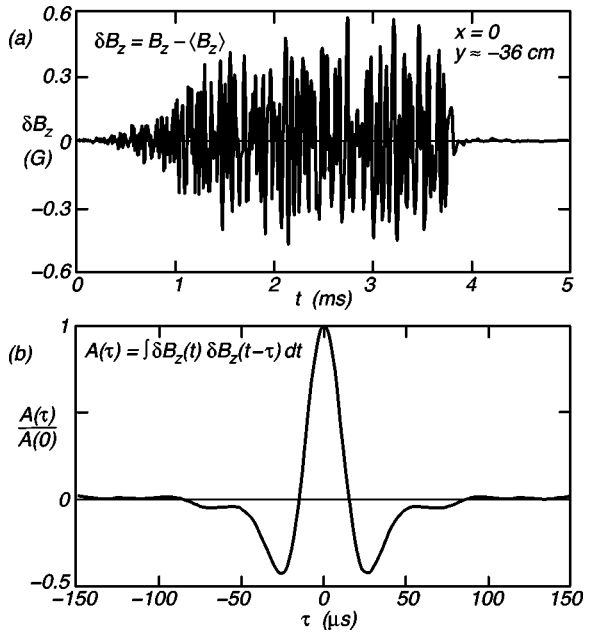

FIG. 8. Field fluctuations detected with a small calibrated magnetic probe. (a) Single-shot trace of $\delta B_z(t)$ showing growth and saturation during the discharge and rapid decay in the afterglow. (b) Autocorrelation function of the magnetic fluctuations showing coherence time $t < 50\ \mu$s.

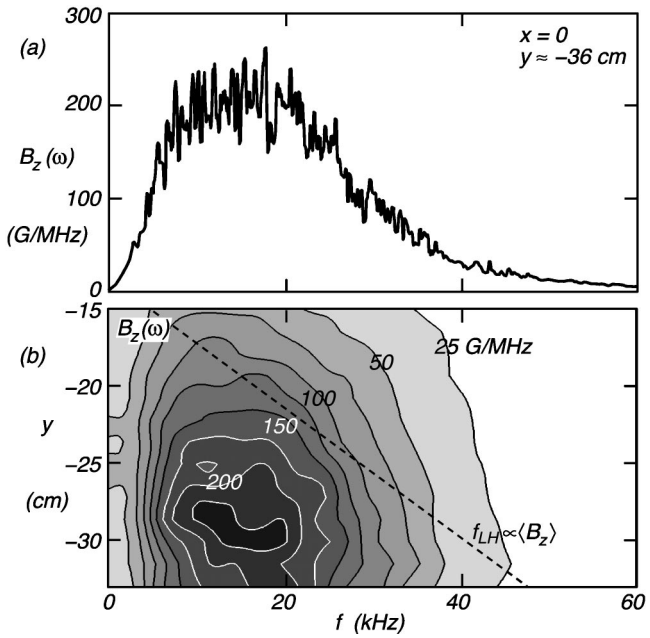

FIG. 9. Frequency analysis of the magnetic fluctuations. (a) Frequency spectrum obtained by a FFT of waveforms as in Fig. 8(b). (b) Contour plot of $\delta B_z(\omega)$ at different radial positions y. The dashed line is the location of the local lower hybrid frequency, $f_{\text{LH}} \propto \langle B_z \rangle(y)$.

the instability ($1.5 \leqslant \tau \leqslant 3.5$ ms). In order to improve the statistics, the correlation is taken over an ensemble of 25 similar time waveforms. One observes that the coherence in time is lost after $\tau \approx 50\ \mu$s, which is just one period of a typical fluctuation. Thus the instability must have a broad frequency spectrum, as is confirmed in Fig. 9.

Figure 9(a) shows a Fast Fourier Transform (FFT) of the magnetic fluctuations, $\delta B_z(\omega)$, during the steady-state period of the discharge for the same waveforms employed in Fig. 8(b). The spectrum exhibits a broad peak at $f \simeq 18$ kHz, but extends to $f \simeq 60$ kHz, which is far below the electron cyclotron frequency at $B_z \simeq 5$ G ($f_{ce} \simeq 14$ MHz), far above the ion cyclotron frequency ($f_{ci} \simeq 175$ Hz), but in the range of the lower hybrid frequency $f_{\text{LH}} \simeq (f_{ci} f_{ce})^{1/2} = 51$ kHz. Since the latter varies with radial position, $f_{\text{LH}} \propto B_z(y)$, the spectrum changes radially as displayed in the contour plot of Fig. 9(b). One observes that toward the column center ($y \rightarrow 0$) the peak in the spectrum shifts to lower frequencies ($B_z \rightarrow 0$). For reference, the lower hybrid frequency at the local magnetic field is indicated by a dashed line. In earlier measurements at higher magnetic fields, the instability has also been observed to occur below but near the lower hybrid frequency.[8] The radial variation of the instability amplitude has already been described in Fig. 7.

C. Plasma afterglow

After the turn-off of the discharge current, the plasma parameters decay, hence the diamagnetism and the instability vanish. These processes are summarized in Fig. 10, which starts with a semilog plot of the electron density and temperature, normalized to their steady-state values in the discharge, at the column center versus afterglow time t_a. The density decays slowest with an e-folding time of τ_n

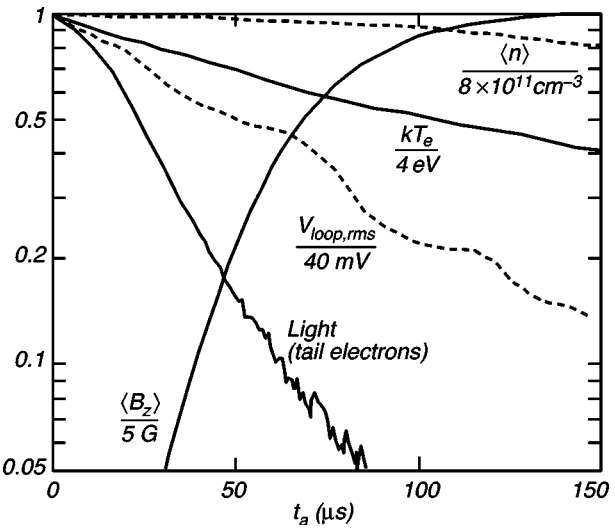

FIG. 10. Decay of plasma parameters and fluctuations in the afterglow. Density decay is slower than electron temperature decay, which in turn is much slower than the loss of light-producing energetic electrons. The axial field recovers ($\langle B_z\rangle \rightarrow B_0$) and the fluctuations decrease with decaying electron energy, although ∇n persists.

$=n/|\partial n/\partial t| \simeq 900\ \mu$s, while the electron temperature decays at a faster rate, $\tau_T = T_e/|\partial T_e/\partial t| \simeq 160\ \mu$s. In a discharge plasma there are also energetic tail electrons ($eV_{\rm dis} \simeq 50$ eV), which produce visible light detected with a photodiode and displayed in Fig. 10. These unconfined electrons decay at the fastest rate, $\tau_{\rm tail} = I_{\rm light}/|\partial I_{\rm light}/\partial t| \simeq 27\ \mu$s. The axial magnetic field in the column center rises from $B_z \simeq 0$ to the ambient field $B_0 = 5$ G at an initial rate comparable to the loss rate of the energetic electrons. The bulk plasma β still exceeds unity at $t = 150\ \mu$s, yet the diamagnetism has essentially vanished. Note that the rise of B_z is delayed in the afterglow ($\sim 30\ \mu$s), which, as shown below, is the result of magnetic field diffusion through the plasma. Finally, the pressure-driven instability, as indicated by the rms fluctuations on the loop voltage, decays at a rate $\tau_{\rm instab} = V_{\rm loop}/|\partial V_{\rm loop}/\partial t| \simeq 74\ \mu$s, which is mainly determined by the electron temperature decay and the magnetic field increase, $v_{\rm dia}/c_s \propto T_e^{1/2}/B_z$, but not by changes in the density gradients.

The decay of the diamagnetism and the fluctuations at different radial positions is shown in Fig. 11. The ensemble-averaged diamagnetic loop voltage, $\langle V_{\rm loop}\rangle(y,t_a)$[Fig. 11(a)], shows that the field rises inside the column [$\langle V_{\rm loop}\rangle(y \simeq 0) > 0$], decays outside it [$\langle V_{\rm loop}\rangle(|y| > 30\ {\rm cm}) < 0$], and that the change in B_z diffuses/propagates from the edge of the plasma column to the center. The observed delay time $\tau_{B_z} \simeq 50\ \mu$s is much faster than the resistive diffusion time $\tau \simeq \mu_0 \sigma_\parallel L^2 \simeq 680\ \mu$s based on the Spitzer conductivity $\sigma_\parallel \simeq 60\ \Omega^{-1}\,{\rm cm}^{-1}$ and radial scale length $L \simeq 30$ cm. The transient EMHD field is likely to be transported by an oblique whistler into the plasma.[25] The net field $\langle B_z\rangle(y,t_a)$ is obtained by integrating the loop voltage and adding the dc magnetic field, and is displayed in Fig. 11(b). Outside the column, the field rapidly decays to $B_0 = 5$ G, while inside the column it rises more slowly to $B_z = 5$ G. The rms fluctuations on the loop voltage maximize off-axis ($|y| \simeq 30$ cm) and decay on a similar time scale as the average magnetic field [Fig. 11(c)]. Nevertheless, at $t \simeq 150\ \mu$s, the normalized plasma pressure at the column center still yields $\beta(0) \simeq 2$, yet instability and diamagnetism have essentially vanished.

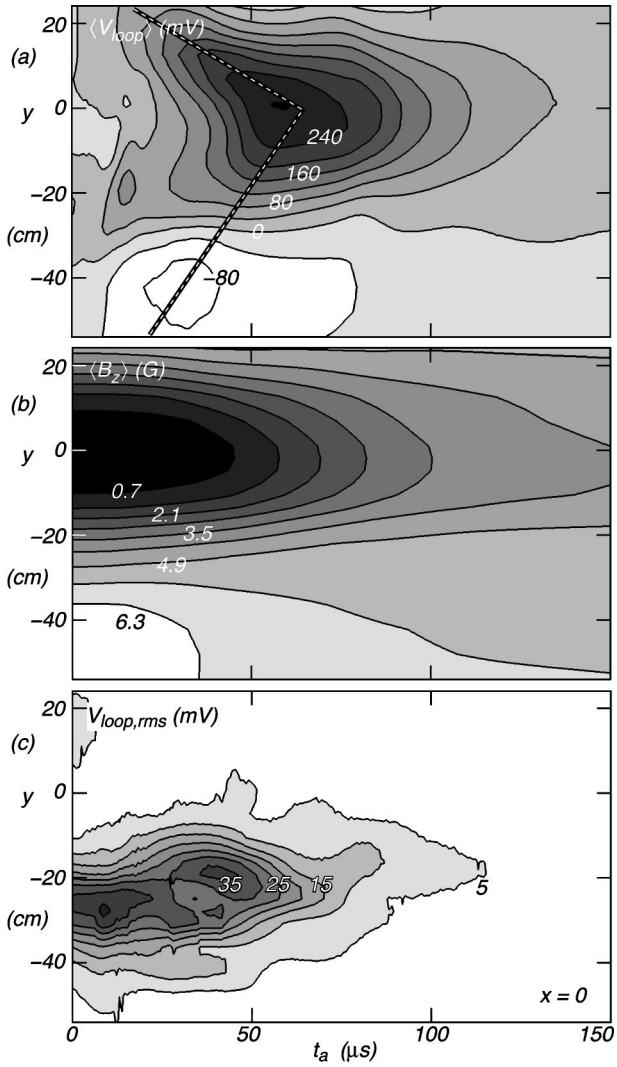

FIG. 11. Decay of mean and rms magnetic fields in the afterglow at different radial positions. (a) Contours of $\langle V_{\rm loop}\rangle(y,t_a)$showing that the field change propagates radially into the plasma. (b) Contours of the average magnetic field $\langle B_z\rangle(y,t_a)$ obtained by subtracting the integrated diamagnetic loop voltage from $B_0 = 5$ G. (c) Contours of magnetic fluctuations ($\propto V_{\rm loop,rms}$), radially peaking near $|\nabla B_z|_{\rm max}$ and decaying at the same rate as the average diamagnetism.

IV. CONCLUSIONS

The properties of a dense discharge plasma in a weak external magnetic field have been measured. The electron diamagnetism expels the field from the plasma interior. In the presence of unmagnetized ions, the electron pressure is balanced by *both* magnetic and electric forces. The pressure balance equation is not applicable and values of plasma $\beta > 1$ are required for complete field expulsion. The cross-field electron drift exceeds the sound speed and drives a strong instability in the region of pressure gradients. Coupled density and magnetic field perturbations are excited near the lower hybrid frequency. The fluctuations propagate in the

direction of the diamagnetic drift but at the much slower sound speed. The saturated instability exhibits short correlation times. In the afterglow plasma, the instability dies out well before the density gradients vanish.

The present observations should be of interest to other plasma configurations with similar parameters. For example, natural magnetic holes have been observed near the magnetopause[5] with strong lower hybrid wave activity at the hole boundary. Although classical pressure balance and the lower hybrid drift instability have been invoked, the present laboratory observations could modify this interpretation. The present results could also apply to other high-β plasmas such as diamagnetic cavities produced in Barium cloud releases in space.[4]

ACKNOWLEDGMENTS

The authors gratefully acknowledge support for this work from National Science Foundation Grant No. PHY 9713240. The authors also thank the anonymous referee for her/his diligence while reviewing this series of papers.

[1]F. F. Chen, *Introduction to Plasma Physics and Controlled Fusion* (Plenum, New York, 1984), Vol. 1, p. 203.
[2]D. Leneman, W. Gekelman, and J. Maggs, Phys. Rev. Lett. **82**, 2673 (1999).
[3]T. J. Dolan, *Fusion Research* (Pergamon, New York, 1982), Vol. 1, p. 34.
[4]P. A. Bernhardt, R. A. Roussel-Dupre, M. B. Pongratz, G. Haerendel, A. Valenzuela, D. A. Gurnett, and R. R. Anderson, J. Geophys. Res. **92**, 5777 (1987).
[5]R. A. Treumann, L. Brostrom, J. LaBelle, and N. Sckopke, J. Geophys. Res. **95**, 19 099 (1990).
[6]D. Longcope, M. Linton, A. Pevtsov, G. Fisher, and I. Klapper, in *Magnetic Helicity in Space and Laboratory Plasmas*, Geophys. Monograph **111**, edited by M. Brown, R. Canfield, and A. Pevtsov (American Geophysical Union, Washington, DC, 1999), p. 93.
[7]A. S. Kingsep, K. V. Chukbar, and V. V. Yankov, in *Reviews of Plasma Physics*, edited by B. Kadomtsev (Consultants Bureau, New York, 1990), Vol. 16, p. 243.
[8]R. L. Stenzel, Phys. Fluids B **3**, 2568 (1991).
[9]N. A. Krall and P. C. Liewer, Phys. Rev. A **4**, 2094 (1971).
[10]R. C. Davidson, N. T. Gladd, C. S. Wu, and J. D. Huba, Phys. Fluids **20**, 301 (1977).
[11]J. D. Huba, A. B. Hassam, and D. Winske, Phys. Fluids B **2**, 1676 (1990).
[12]A. J. Hayzen and P. J. Barrett, Phys. Fluids **20**, 1713 (1977).
[13]J. D. Huba, Geophys. Res. Lett. **20**, 2763 (1993).
[14]W. Horton, Rev. Mod. Phys. **71**, 735 (1999).
[15]B. B. Kadomtsev, *Plasma Turbulence* (Academic, New York, 1965), p. 96.
[16]J. A. Shercliff, *A Textbook of Magnetohydrodynamics* (Pergamon, New York, 1965), p. 69.
[17]J. M. Urrutia and R. L. Stenzel, Phys. Plasmas **7**, 4457 (2000).
[18]R. L. Stenzel and J. M. Urrutia, Phys. Plasmas **7**, 4465 (2000).
[19]R. L. Stenzel and W. F. Daley, United States Patent No. 4,216,405, August 5, 1980.
[20]R. L. Stenzel, Phys. Fluids **21**, 93 (1978).
[21]R. L. Stenzel, Phys. Fluids **21**, 99 (1978).
[22]R. L. Stenzel, Phys. Fluids **19**, 857 (1976).
[23]S. C. Brown, *Basic Data of Plasma Physics* (Wiley, New York, 1959), p. 7.
[24]R. L. Stenzel, J. Geophys. Res. **82**, 4805 (1977).
[25]J. M. Urrutia, R. L. Stenzel, and C. L. Rousculp, Phys. Plasmas **2**, 1100 (1995).